Dalton Transactions

ROYAL SOCIETY OF CHEMISTRY

PAPER

View Article Online
View Journal | View Issue

Check for updates

Cite this: *Dalton Trans.*, 2024, **53**, 9516

Triptycene as a scaffold in metallocene catalyzed olefin polymerization†

Pavel S. Kulyabin, [a] Mikhail I. Sharikov,[a] Vyatcheslav V. Izmer,‡[a] Dmitry S. Kononovich,[a] Georgy P. Goryunov, [a] Nikita V. Alexeev, [a] Dmitry V. Uborsky, [a] Antonio Vittoria, [b] Giuseppe Antinucci,[b] Christian Ehm, [b] Peter H. M. Budzelaar,*[b] Roberta Cipullo, [b] Vincenzo Busico *[b] and Alexander Z. Voskoboynikov *[a]

Received 22nd April 2024,
Accepted 10th May 2024

DOI: 10.1039/d4dt01170h

rsc.li/dalton

A set of metallocene olefin polymerization catalysts bearing triptycene moieties in either position 4–5 (complexes **Ty1–Ty5**) or in position 5–6 (complexes **Ty6–Ty8**) of the basic dimethylsilyl-bridged bis(indenyl) system has been tested in propene polymerization and in ethene/1-hexene copolymerization. Comparison of the results with QSPR (quantitative structure–property relationship) predictions not parametrized for these exotic ligand variations demonstrates that trends can still be identified by extrapolation. Interestingly, **Ty7**, upon suitable activation, provides a highly isotactic polypropylene with an exceptional amount of 2,1 regio-errors (8%). The previously developed QSPR type models successfully predicted the low regioselectivity of this catalyst, despite the fact that the catalyst structure differs significantly from the benchmark set.

Introduction

Catalysis of olefin polymerization is all about control: control of stereochemistry,[1–7] of regiochemistry (1,2 *vs.* 2,1 insertion),[8–11] of molecular weight (insertion *vs.* β-H transfer and hydrogenolysis),[2,12–15] of chemoselectivity (ethene *vs.* propene *vs.* α-olefins),[16–20] of catalyst stability (propagation *vs.* deactivation),[21–24] and catalyst activity.[25–28] For typical catalyst classes the main factor is sterics.[29,30] Stereoselectivity is completely determined by steric interactions between ligand, growing chain and incoming monomer.[29,30] Regioselectivity and chemoselectivity have some contributions from electronic factors but are still dominated by sterics.[16,17,31,32] Electronic factors are more relevant in MW (molecular weight) control.[33] Thus, it stands to reason that catalyst optimization (within a given class) is a matter of precision tuning of the catalyst 3D structure. Enzymes achieve this kind of finetuning through their tertiary structure, which is mostly held together by hydrogen bridges.[34,35] Human design of the 3D structure of polymerization catalysts cannot use this principle, if only because hydrogen bridges are acidic and would not survive in the alkylating medium of a polymerization reaction.[27] One could imagine ligand structure being precisely architected using non-covalent interactions,[36] but the art of ligand design has not yet progressed to the point where this is practical. Moreover, the approach seems ill suited for the high operating temperatures employed in industrial olefin polymerization (T_p > 100 °C). Thus, we must instead rely on covalent linking of building blocks, and this imposes severe limitations on the design of 3D structures. The importance of catalyst rigidity in olefin polymerization is well-documented,[13,32,37–39] but achieving such rigid structures precisely covering the right distribution of steric bulk over space is nontrivial. Enforced coplanarity of catalyst fragments (*e.g.*, cyclopentadienyl (Cp) → indenyl) is relatively easy to establish. Orthogonal connections (*e.g.*, aryl – 2,6-$Me_2C_6H_3$) are also easy to enforce, be it that usually some flexibility remains. Unrestricted connections (bonds having free rotation) are straightforward. For anything more complex than these, sophisticated and creative choices of building blocks are required. This is nicely illustrated by our recently reported two metallocene catalysts bearing triptycyl fragments in their skeleton, with the 9,10-dihydroanthracenyl moieties bridging the indenyl positions 4 and 5 (**Ty1** and **Ty2** in Fig. 1).[13]

In these complexes the ligands precisely cover space around the metal center to virtually suppress stereo- and regioerror insertion as well chain end epimerization and β-H transfer to monomer, thus providing highly regioregular isotactic poly-

[a]*Department of Chemistry, Lomonosov Moscow State University, 119991 Moscow, Russia. E-mail: voskoboy@med.chem.msu.ru*
[b]*Dipartimento di Scienze Chimiche, Università di Napoli Federico II, 80126 Napoli, Italy. E-mail: p.budzelaar@unina.it, busico@unina.it*

†Electronic supplementary information (ESI) available: Synthesis of proligands, NMR spectra of synthetic intermediates and metal complexes, full polymerization results, details for the QSPR models and DFT calculations. CCDC 2308227. For ESI and crystallographic data in CIF or other electronic format see DOI: https://doi.org/10.1039/d4dt01170h

‡Deceased

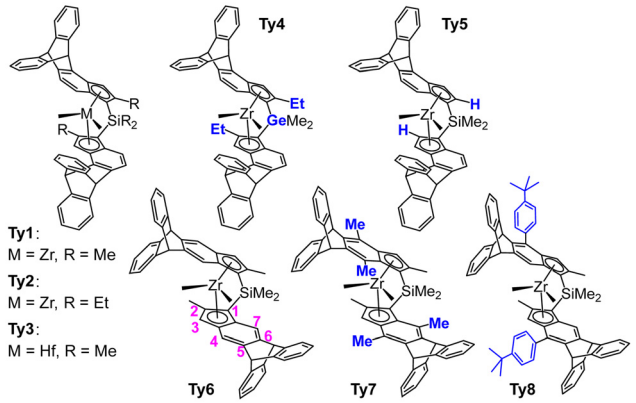

Fig. 1 Triptycene based metallocenes tested in olefin polymerization catalysis. **Ty1–Ty5**: 4,5-bridged, **Ty6–Ty8**: 5,6-bridged. Modifications relative to the parent compounds **Ty1** and **Ty6** indicated in blue. Numbering of indenyl positions in magenta. **Ty1/Ty2**,[13] **Ty3**,[40] **Ty4–Ty8** this work.

propylene with a high molecular mass capability. This precision architecture was made possible by the unusual paddle-wheel shape of the triptycyl unit,[41] which allows fixing of ligand fragments at 120° angles. The relative rigidity of the resulting ligand backbone presumably is also an important factor.[13]

We consider the prediction[13] of superior performance of catalysts **Ty1** and **Ty2** a success of our QSPR (quantitative structure–property relationship) type modelling.[12,29,31,32] In order to broaden the applicability of our model in the future, covering aspects of catalyst structures not taken into account in the training set used to predict **Ty1** and **Ty2** performances, we embarked on the synthesis, although demanding, of several new triptycyl complexes (Fig. 1):

(a) **Ty3**, the Hf analog of **Ty1**, features a different central metal (Hf *vs.* Zr),[37]

(b) **Ty4** features a variation of the metallocene bridge atom (Ge *vs.* Si) with respect to **Ty2**.

(c) **Ty5** lacks the crucial 2-*R*-substituent, which is present in **Ty1** and **Ty2**.

(d) **Ty6–8** incorporate a 5,6 instead of 4,5 bridging triptycyl unit. Note that **Ty7** shows in addition severe distortions of the ligand framework introduced by 7-Me substituents.

In this manuscript we report on the synthesis of the metallocenes of Fig. 1 and on their performance in propene polymerization and ethene/1-hexene copolymerization. Predictions by QSPR models are also discussed.

Results and discussion

Synthesis of metallocenes

We have developed a strategy for the synthesis of triptycene derived metallocenes that is quite general and requires in most cases easily available starting materials: variously halogenated toluenes or indanones. No evidence for a specific "triptycyl effect" has been observed. Triptycene moieties have been incorporated in sophisticated ligand frameworks in different ways, such as: (a) connected at C9 as a very bulky C_3-symmetric *t*-alkyl substituent for Tpz type ligands,[42] (b) acting as a spacer for wide-angle bidentate diphosphine ligands in hydroformylation,[43,44] (c) attached at C1 as a very bulky and asymmetric aryl substituent at the N atoms of NHC ligands,[45] (d) as an aromatic scaffold for mono-and dinucleating diphosphinamide ligands for ethene oligomerization.[46]

Syntheses of metallocenes **Ty1–3** was described in our preceding papers.[13,40] Proligands for new 4,5-bridged triptycene precatalysts **Ty4** and **Ty5** were synthesized using the same malonate pathway, only differing in the reactants used: Me_2GeCl_2 for **Ty4** and diethyl malonate for **Ty5** (Scheme 1).

The key step in the synthesis of indenes with 5,6-bridged triptycene moieties was the Diels–Alder reaction of the benzyne formed from the respective 5,6-dihalogen-substituted methoxyindanes Scheme 2). The *ortho*-dihalogen-substituted aryl moiety was either in the starting compound (**6a**) or introduced by bromination (**7a** to **7b**) or diazotation (**8a** to **8b**). After elimination of methanol from the intermediate methoxyindanes, the indenes thus obtained were converted to the Me_2Si-

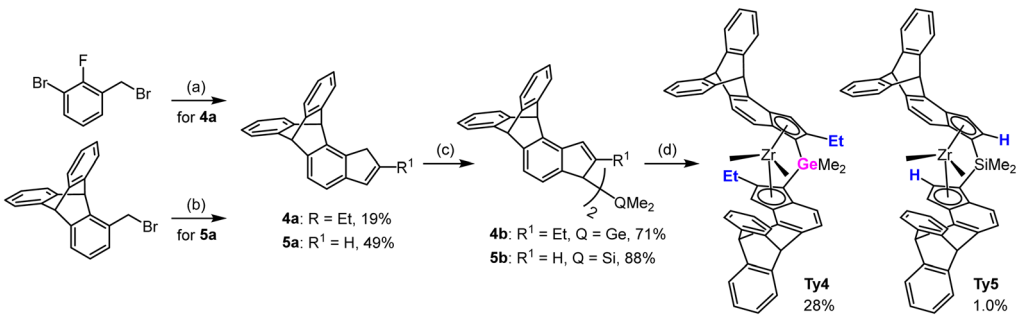

Scheme 1 Syntheses of 4,5-bridged triptycene precatalysts. (a) see ref. 13 (b) 1. NaH, $CH_2(COOEt)_2$, THF; 2. KOH, water, reflux; 3. HCl_{aq}; 4. 160 °C; 5. H_3PO_4-P_4O_{10}, 130 °C; 6. $NaBH_4$, MeOH-THF; 7. TsOH, PhMe, reflux; (c) for **4b**: i. *n*BuLi, Et_2O, ii. Me_2SiCl_2, *N*-methylimidazole; for **5b**: *n*BuLi, Et_2O, ii. CuCN, Me_2SiCl_2. (d) for **Ty4**: 1. i. *n*BuLi, Et_2O, ii. $ZrCl_4$; 2. MeMgBr, PhMe-Et_2O; 3. LiCl, THF; for **Ty5**: 1. i. *n*BuLi, Et_2O, ii. $ZrCl_4$; 2. *rac*/*meso* separation, 3. MeMgBr, Et_2O.

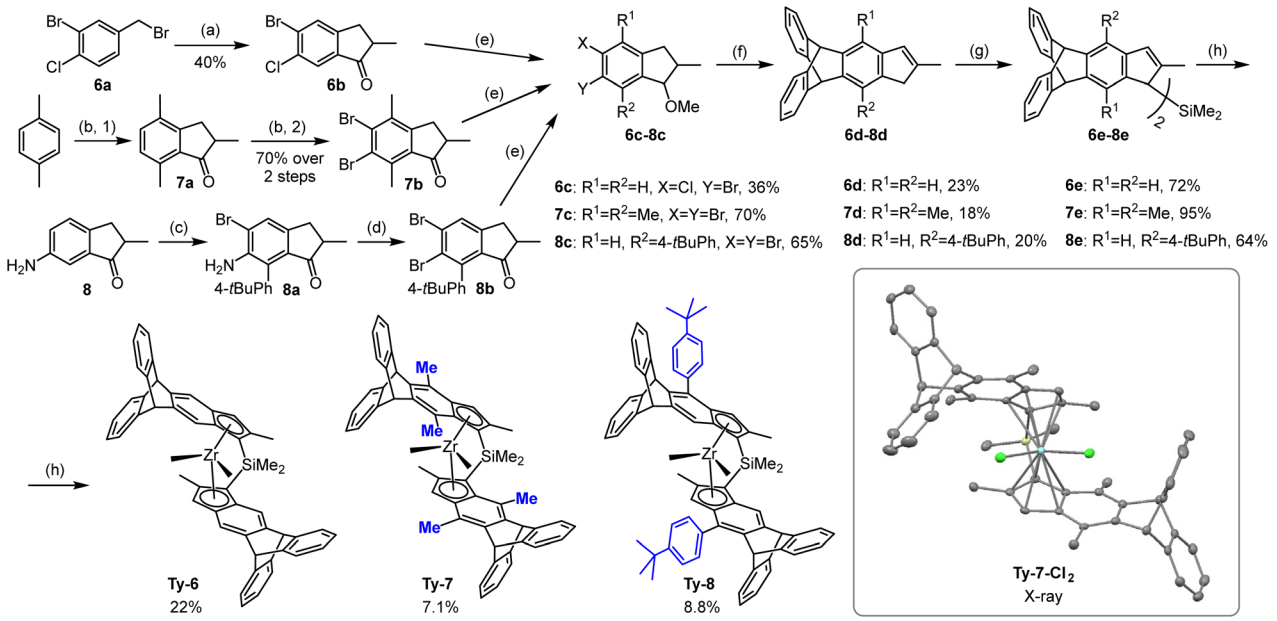

Scheme 2 Syntheses of 5,6-bridged triptycene precatalysts: (a) 1. $MeCH(COOEt)_2$, NaOEt, EtOH 2. KOH, water, reflux; 3. 180 °C; 4. $SOCl_2$, CH_2Cl_2; 5. $AlCl_3$, CH_2Cl_2. (b) 1. $AlCl_3$, CH_2Cl_2; 2. one-pot: Br_2, CH_2Cl_2. (c) 1. NBS, DMF; 2. 4-*t*BuPhB$(OH)_2$, Cs_2CO_3, $Pd(PPh_3)_4$, dioxane/water, reflux; 3. NBS, DMF. (d) amyl nitrite, $CuBr_2$, MeCN. (e) 1. $NaBH_4$, MeOH-THF; 2. for **6c**, **7c**: KOH, MeI, DMSO; for **8c**: NaH, MeI, THF. (f) 1. *n*BuLi, THF, anthracene, 2. for **6d**: HCl (aq.), MeOH, reflux; for **7d**, **8d**: TsOH, PhMe, reflux. (g) For **6e**, **7e**: i. *n*BuLi, Et_2O, ii. THF, CuCN, Me_2SiCl_2; for **8e**: i. *n*BuLi, Et_2O, ii. Me_2SiCl_2, *N*-methylimidazole (h) i. *n*BuLi, $ZrCl_4$, Et_2O; ii. *rac*/*meso* separation; 3. MeMgBr, Et_2O. Insert: crystal structure of **Ty7-Cl$_2$**: image generated by Mercury software with thermal ellipsoids at 50% probability level; hydrogen atoms and co-crystallized toluene molecules omitted for clarity.

bridged proligands *via* reaction of their lithium salts with Me_2SiCl_2 in the presence of CuCN or *N*-methylimidazole.[47]

Most of the racemic dimethyl complexes (**Ty5–Ty8**) were obtained by reaction of the racemic dichloride precursors (separated from the isomeric *meso* side-products by crystallization in the previous step) with MeMgBr. For preparation of Me_2Ge-bridged **Ty4**, we used LiCl-catalyzed isomerization of a mixture of dimethyl complexes *rac*/*meso*-**Ty4** to the *rac*-**Ty4**,[47] which was then isolated by crystallization.

The crystal structure of **Ty7-Cl$_2$**, the dichloride precursor of **Ty7**, was elucidated by X-ray diffraction analysis. The asymmetric unit cell contains two molecules of co-crystallized toluene, located on left side with respect to the plane bisecting the left and right halves of the structure (inset in Scheme 2 and Fig. S1†) thus distorting the ligand surrounding in the respective area of the metallocene and the overall C_2-symmetry of the complex.

Ty7-Cl$_2$ has methyl groups at indenyl position 7, a feature for which there are relatively few examples in the literature. Repulsion between position 7 substituents and neighboring Si–Me groups affects the entire structure in a number of common ways:[37,48,49] (1) the 7-methyls are pushed from the mean planes of the benzene rings they are connected to by 0.450/0.355 Å; (2) the Si–Me groups are pushed to the opposite direction resulting in rotation of the Me–Si–Me plane with respect to the Cl–Zr–Cl plane (torsion angles Me–Si–Zr–Cl are 10.85/10.30° *vs.* 1.36/1.64° in **Ty1**[13]); (3) the ligand bite angle is reduced (57.58° *vs.* 59.54° in **Ty1**); (4) the Cp moieties are rotated with respect to each other (angle C2–Cp_{cent}–Cp_{cent}′–C2′ is 8.64° *vs.* 1.98° in **Ty1**); (5) the Zr–C_{Cp} distances change: *e.g.* Zr–C1/C1′ are elongated (2.618/2.599 *vs.* 2.583/2.576 Å in **Ty1**), whereas Zr–C3/C3′ are shorter (2.488/2.476 *vs.* 2.534/2.532 Å in **Ty1**).

Testing in iPP catalysis

The new metallocenes **Ty4–Ty8** were tested in our high-throughput experimentation setup (described in detail in ref. 50 and 51) in propene polymerization at T_p = 60 °C and $p_{propene}$ = 6.6 bar, as well as at T_p = 100 °C and $p_{propene}$ = 7.9 bar, where possible. Conditions were held rigorously identical to those used previously for **Ty1**/**Ty2**,[13] and **Ty3**,[40] so numbers cited allow direct comparison. Results for the new catalysts **Ty4–Ty8** are summarized in Table 1, together with data for previously studied systems (**Ty1–Ty3**) included here for comparison. It should be noted that the employed protocol emphasizes kinetic control over catalyst activity utilizing an activation delay to minimize undesired effects on polymer properties.[52] Activities (see ESI†) are therefore not representative of the maximum activities attainable for these catalysts.

Both **Ty1** and **Ty2** feature remarkable stereoselectivity (even at elevated temperature) as well as good regioselectivity, high MW and good activity, as reported earlier. **Ty3**, which differs from **Ty1** in the central metal (Hf *vs.* Zr), shows similar stereoerrors, higher molecular weight and higher regioselectivity. At elevated temperatures (T_p = 100 °C), both stereoselectivity and molar mass capability of **Ty3** are lower than with **Ty1** (see ESI†).

Ty4, which was synthesized to test the influence of a germanium-based bridge, shows similar performance to **Ty2** in terms of regio- and stereoselectivity at T_p = 60 °C; the molar

Table 1 Summary of the characterization results of PP samples obtained with catalysts **Ty1–Ty8**

	60 °C					100 °C				
Catalyst	$1-\sigma$, %	2,1, %	3,1, %	M_n, kDa	PDI	$1-\sigma$, %	2,1, %	3,1, %	M_n, kDa	PDI
Ty1	≤0.02	0.26	n.d.	1100	2.5	0.03	0.33	0.02	200	2.1
Ty2	0.03	0.18	n.d.	1900	2.1	0.04	0.23	0.03	140	2.3
Ty3	0.03	0.11	n.d.	1400	2.3	0.10	0.12	0.06	90	2.0
Ty4	≤0.02	0.19	n.d.	880	2.6	≤0.02	0.24	0.03	150	2.5
Ty5	0.05	1.0	n.d.	60	2.1	not tested, molar mass capability too low				
Ty6	1.2	1.3	0.05	40	2.0					
Ty7	0.43	7.9	0.1	25	2.0					
Ty8	0.03	1.3	0.02	430	2.1	0.10	1.4	0.48	67	2.1

Other experimental conditions: solvent, toluene; scavenger/activator, tri-*iso*-butylaluminum/$HNMe_2Ph^+[B(C_6F_5)_4]^-$ (TIBA/AB). Propene pressure at 60 °C: 6.6 bar, at 100 °C: 7.9 bar. All data are averages of at least duplicate experiments. n.d. not detected. For further details see ESI.†

mass capability is similar. However, at elevated temperatures, the catalyst appears to be unstable, which might explain why despite initial promising reports by Kaminsky,[53] Ge-based bridges have not attracted attention in the field. **Ty5** lacks a substituent at indenyl position 2. This substitution is generally considered to be a requirement for obtaining decent MW.[54] Our results support this, as illustrated by the observed MW for **Ty1** that is 20 times higher than for **Ty5**.

The performance of the new 5,6-bridged systems **Ty5–Ty8** differs dramatically from the 4,5-bridged systems studied before. This should not be too surprising: while use of the 4,5-bridged skeleton apparently puts steric bulk exactly where it is most effective, the use of the 5,6-linker creates bulk in a different and presumably less effective region of space. This is precisely why we want to include such sub-optimal species in our future model building.

In fact, the introduction of the 5,6-triptycene unit in **Ty6** even lowers the molar mass capability compared to the parent 2-Me-indenyl *ansa*-metallocene,[12] even though substituents at the positions 5 and 6 are known to increase molar mass capability.[31,32,55] In **Ty8**, *stereo*selectivity is restored to the level of **Ty1** by the addition of a bulky aryl group at the indenyl position 4 while molar mass capability is mostly but not fully restored.

Evidently, only the simultaneous introduction of substituents at the positions 4 and 5–6 constrains the active pocket enough to affect chain transfer transition states, and the 5,6-triptycene unit appears to be roughly as effective as a 6-Ph substituent in increasing molar mass capability.[31] In contrast, regioselectivity of **Ty8** is *not* restored to the **Ty1** level.

Ty7 is, from a scientific point of view, the most interesting new catalyst. Fig. 2 reports the ^{13}C NMR spectrum of a polypropylene obtained a 60 °C with **Ty7**. In addition to the three main resonances typical of a regioregular polypropylene,[2] the set of resonances ascribed to the head-to-head/tail-to-tail enchainments are well visible.[2] Interestingly the resonances of 3,1 units are hardly visible (<0.1%), suggesting that isomerization of a last 2,1 propene insertion is still blocked for **Ty7** like it is for **Ty1**/**Ty2**.

The expansion of the methyl region of the ^{13}C NMR spectrum (Fig. 2) clearly shows that the sample is highly stereoregular, since the intensity of the peak at 19.7 ppm due to the isolated stereoerror is lower than that of the ^{13}C–^{13}C satellite band of the main resonance (marked with an asterisk). Overall, **Ty7** produces, to our knowledge, an unprecedented polypropylene sample with an exceptionally *high* degree of regiodefects in the form of isolated 2,1 units: 7% (with only ~0.4% stereoerrors). Typical values for *e.g.* Spaleck-type selectivity would be <1% stereo-errors and 1–2% 2,1e regiodefects.[56] Resconi[56–58] has reported up to 3.4% 2,1 regioerrors in polymers produced with *rac*-Me_2Si(2-Me-4-Ph-5-OMe-6-*t*Bu-Ind)$_2ZrCl_2$.[55] The regioselectivity and 3,1-isomerization tendency of this catalyst is however tied to activation/immobiliz-

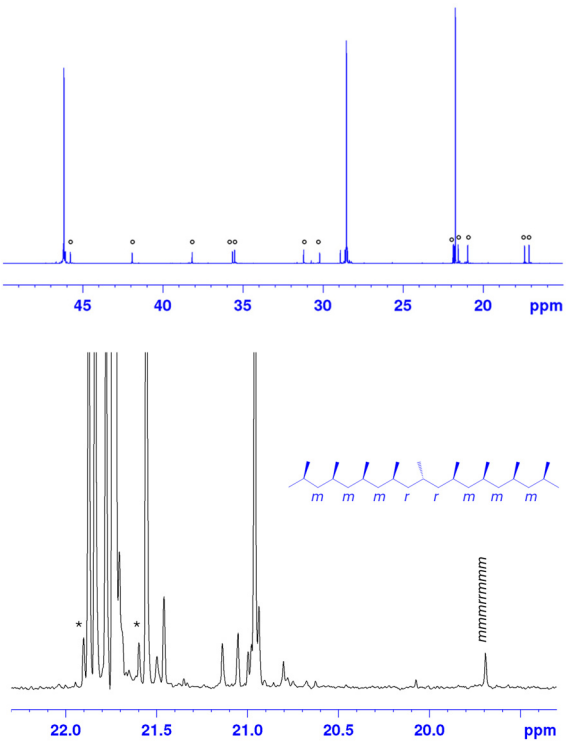

Fig. 2 Full ^{13}C NMR spectrum (top) and expansion of the methyl region (bottom) of highly regioirregular iPP made using catalyst **Ty7**. Peaks marked with * and o are due ^{13}C–^{13}C satellite band and to regioerrors, respectively.

Table 2 Reactivity ratios for catalysts **Ty1–Ty8** in ethene/1-hexene polymerization at 60 °C

Catalyst	r_E	r_H
Ty1	4.0	0.23
Ty2	3.5	0.23
Ty3	3.3	0.25
Ty4	4.4	0.21
Ty5	3.4	0.27
Ty6	8.8	0.014
Ty7	19	0.12
Ty8	3.3	0.29

ation conditions.[31,57] This opens the door to study the effect of the presence of substantial amounts of 2,1 units in stereoregular polypropylene samples on material properties. On this we will report in due time.

Testing in ethene/1-hexene copolymerization catalysis

All catalysts were also tested in ethene/1-hexene copolymerization under standard conditions previously used for database building.[17] Comonomer feeding ratio was adjusted to obtain copolymers with high 1-hexene incorporations to evaluate from a single ^{13}C NMR spectrum the reactivity ratios values (see ESI† and Experimental section). Table 2 summarizes the r_E and r_H values, averaged on at least duplicate experiments.

For the catalysts with considerable steric bulk around the active pocket, **Ty1–Ty5** and **Ty8**, the comonomer affinity after ethene insertion is on par with the best performing C_2-symmetric *ansa*-metallocene catalysts identified recently in a large screening (r_E 3.2–4.6).[59] Similarly, the comonomer affinity after 1-hexene insertion (r_H = 0.21–0.29) is comparable to other *ansa*-metallocenes.

For the 4,5-triptycenes (**Ty1–4**), the reactivity ratios values are insensitive to changes in substituent pattern, and metal changes (**Ty1** *vs.* **Ty3**). This has been rationalized previously as indicative of a change in rate limiting step from insertion to olefin capture,[17,20] which is typical for well performing catalysts of this class. The effects of the 5,6-triptycene pattern, notable in propene polymerization, are minimal with respect to the comonomer affinity. Only **Ty6** and **Ty7**, which are also the worst performing catalysts in propene polymerization, show poorer comonomer affinity (higher r_E and lower r_H value). However, their performance is similar to that of their parent metallocene system[17] (2-Me-indenyl)$_2$SiMe$_2$ZrCl$_2$, and (2-4-di-Me-indenyl)$_2$SiMe$_2$ZrCl$_2$, respectively.

How effective are QSPR predictions?

Catalysts **Ty1** and **Ty2** were "designed" based on a QSPR model built using many standard metallocene catalysts, none of which had any "exotic" substituents like the triptycyls discussed here.[13,31] It was clear from the start that this reported model would not be capable of producing *quantitatively* accurate predictions for these new catalysts (nor for the remaining species **Ty3–Ty8**). However, it was good enough to guide us in the synthesis of the metallocenes **Ty1** and **Ty2** which showed unprecedented high-temperature performance.

To understand if it was just a lucky coincidence or the model, although based on incomplete data set structures, can nevertheless help prioritize the search for new catalyst types, it is instructive to confront the experimental data for these triptycyl-bearing catalysts with the relevant predictions (Table 3).

Predictions for catalysts **Ty1–Ty2** and **Ty8**, bearing some resemblance to the catalysts used to build the QSPR models, are in good agreement with the observed experimental performance, especially for stereoselectivity. Regioselectivity (measured as regio$_{tot}$, *i.e.* the total sum of all regioerrors) and molar mass capability, in terms of number average molecular weight, M_n, deviate up to a factor of 2–4 from the predictions, which isn't much in terms of absolute energy differences (RT ln 2 = 0.5 kcal mol^{-1} at 333 K). Moreover, for these catalysts the reactions are very challenging to control at such a low polymerization temperature, and the uncertainty in the experimental data for molar mass capability is therefore substantial.[40]

Conversely **Ty3–Ty7** incorporate more drastic changes, for which no training was done whatsoever, *e.g.*, changes in central metal or bridging element, and lack of 2-*R* or 4-*R* substituent. However, stereoselectivity predictions are in relatively good agreement with experiment, with deviations not exceeding a factor of ≈2.

Qualitatively, predictions for **Ty3** (Hf) and **Ty4** (Ge) regioselectivity and molar mass capability are good; however, the predicted direction of the Hf-effect (decreasing regioselectivity) is wrong,[40] as is the Ge-effect (no effect observed but regioselectivity increase predicted). This isn't surprising: the models were build relying exclusively on silyl bridged zirconocenes. In the grand scheme, this calls into question the applicability of the electronic descriptor e^-_{NPA,MCl_2} (NPA charge on the MCl_2 fragment) for across-the-board models.

The substituent pattern changes in **Ty5** (missing 2-*R* substituent) and **Ty6** (missing 4-*R* substituent) challenge especially the molar mass capability model. Molar mass capability is overestimated by a factor of 220 for **Ty5** and a factor of 15 for **Ty6**. The linear QSPR models we have developed treat substituent effects as additive, essentially reflecting the gradual evolution in catalyst development. For example, since the discovery of the 2-Me effect,[54] there was no reason to go back to 2-H systems. The disagreements could indicate that only the simultaneous steric pressure from two sides induces effects, for that

Table 3 Observed *vs.* predicted performance of catalysts **Ty1–Ty8** in propene polymerization at T_p = 60 °C, $p_{propene}$ = 6.6 bar

	$1-\sigma$, %		*regio*$_{tot}$ %		M_n, kDa	
Catalyst	Obs.	Pred.	Obs.	Pred.	Obs.	Pred.
Ty1	≤0.02	≤0.02	0.26	0.11	1100	2700
Ty2	0.03	≤0.02	0.18	0.08	1900	2500
Ty3	0.03	≤0.02	0.11	0.19	1400	2200
Ty4	≤0.02	≤0.02	0.19	0.06	880	4400
Ty5	0.05	≤0.02	1.0	0.1	60	13 000
Ty6	1.2	1.75	1.35	1.82	40	580
Ty7	0.43	0.92	7.9	22.8	25	350
Ty8	0.03	0.04	1.32	0.77	430	2100

without one of the "anchors", the space demanding β-hydrogen transfer to monomer TS can simply escape in one direction. From a model building perspective, this indicates that "if/then" situations might exist and should be incorporated into the models. Alternatively, electronic factors could dominate for these catalysts which are unimportant in the training set and therefore not considered in the molar mass QSPR model. Indeed, **Ty5** is much less electron-poor than the other Ty catalysts and the catalysts in the training set of the QSPR model (e^-_{NPA,MCl_2} 0.343 *vs.* 0.38–0.42 for other Ty catalysts and metallocenes in the training set).

The 7-Me substituents in **Ty7**, not present in the original *ansa*-zirconocene training set, significantly distort the catalyst backbone, something not present in the original *ansa*-zirconocene training set. The molar mass capability model fails for **Ty7** but the regioselectivity model reproduces the very low regioselectivity fairly well (22.8 *vs.* 8.0 mol% $regio_{tot}$), considering that the performance is significantly outside of the model training set (max. 1.4 mol%). Importantly, based on the model we can trace the origin of this peculiar regioselectivity to an increased steric bulk in the open quadrant originating from the distortion of the relative positions of the indenyl fragments (Fig. 3) due to the 7-Me substituents.

Due to the backbone distortion, the 4-Me substituent moves partially into the open quadrant interfering with the 1,2-insertion transition state, while 2,1 insertion transition state is almost unaffected. Salan-type catalysts with very bulky *ortho*-substituents show decreased regioselectivity for similar reasons.

As a side note, the isomerization of 2,1 to 3,1 units requires β-hydrogen elimination from the CH_3 unit, rotation, and reinsertion.[2] DFT calculations (for details see ESI†) indicate that unproductive β-hydrogen elimination from the CH_2 unit is preferred over elimination from the CH_3 unit leading to 3,1-isomerization by $\Delta\Delta G^{\ddagger}$ = 8.1 kcal mol^{-1}, explaining why for **Ty7** "all" regioerrors are present the form of head-to-head/tail-to-tail enchainments.

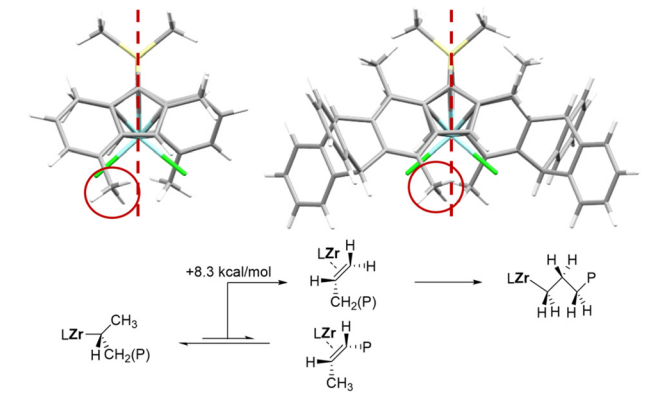

Fig. 3 Top: change in relative orientation of the indenyl fragments repositions the 4-Me substituents. Comparison of *rac*-Me_2Si(2-Me-4-Me-indenyl)$_2ZrCl_2$ and **Ty7**. The resulting interference with 1,2 transition states is responsible for the low regioselectivity of **Ty7**. Red dashed lines indicate the middle plane of the active pocket, separating the two active sites. Bottom: the two possible β-hydrogen eliminations after 2,1 insertion in **Ty7**.

Interestingly, the QSPR predictions for the copolymerization reactivity ratios r_E and r_H are much more effective (see ESI†). However, as some of us have previously shown, likely, insertion is not rate limiting in most of these cases and changes in the active pocket therefore have much smaller, if any, effects on these parameters.[17,20]

Conclusions

In conclusion, we report on the synthesis of several exotic triptycyl complexes and on their performance in propene polymerization and ethene/1-hexene copolymerization. Installing a triptycene motif in position 5,6 deteriorates the catalyst performance in propene polymerization with respect to the 4,5 analogues, but not in ethene/1-hexene copolymerization. The comparison between experimental results and predictions based on QSPR models built using standard metallocene catalysts shows that, as expected, the main performance indicators are not always quantitatively reproduced. However, this shouldn't be surprising; several of the tested triptycene catalyst features are far outside the original training set such as metal changes, missing *R*-substituents, or significant distortions. However, the models can qualitatively predict the performance for modestly "extrapolating" candidate catalysts. This is the case, for example for **Ty7**, producing an isotactic polypropylene with an unprecedent high level of 2,1-insertions.

The continuing interest in this topic ensures we will keep on improving our understanding of the intimate details of olefin polymerization. QSPR type model building can be a useful tool in this effort, in favourable cases pointing us to interesting effects we might not have found solely through inspired substituent choices. To broaden the applicability of QSPR type models, experimental databases need to be grown that also cover unusual substituent patterns. Importantly, metal changes are ill reproduced by current models, indicating that electronic descriptors need to be identified that describe electronic effects of the ligand framework and differences in central metal equally well. The development of improved models applicable to more than one catalyst class/central metal will critically depend on the identification of such descriptors.

Experimental

Inorganic synthesis

The synthesis of zirconocenes **Ty4–Ty8** is detailed in the ESI.† The synthesis of **Ty1**,[13] **Ty2**,[13] and **Ty3**[40] has been reported before. Starting compounds 1-(bromomethyl)triptycene,[13] 2-ethylcyclopenta[*a*]triptycene (**2**),[13] 6-amino-2-methylindanone (**8**),[60] were prepared according to literature procedures. Ethereal solvents were distilled from sodium/benzophenone. Toluene and hexane were sparged with argon and

dried over molecular sieves 4 A. Other reagents were purchased from commercial sources and used as received. All manipulations with compounds, which are sensitive to moisture and air, were performed either in an atmosphere of argon using a standard Schlenk technique or in an inert atmosphere (Ar) of glove box (MBraun). GC/MS analysis was performed on Agilent Technologies 7890A paired with Agilent Technologies 5975C MSD GC/MS system and on Agilent Technologies 8890 GC/5977C MSD system. High-resolution mass spectra (HRMS) were recorded on an Agilent Technologies 6530 Q-TOF LC/MS system paired with Agilent 1260 HPLC and using Agilent JetStream ion source. NMR spectra were recorded on Bruker AVANCE (400 MHz) or Agilent Technologies 400-MR (400 MHz) NMR spectrometers and can be found in the ESI.† C, H, N microanalyses were done using PerkinElmer 2400 Series II CHNS/O elemental analyzer.

X-ray crystallography

X-ray experiments were carried out using Bruker D8 Quest with Photon III detector diffractometer (λ(Mo-Kα) = 0.71073 Å, graphite monochromator, ω-scans) at 100 K. The structure was solved by direct methods and refined by the full-matrix least-squares procedure in anisotropic approximation for non-hydrogen atoms. All hydrogen atoms were placed in geometrically calculated positions and included in the refinement using riding model. The details of data collection and crystal structure refinement for which we used SAINT Plus,[61] SADABS[62] and SHELXL-2018/3[63] program packages, are summarized in Table S1.† The crystallographic data for **Ty7-Cl$_2$** has been deposited with the Cambridge Crystallographic Data Center, CCDC 2308227† (**https://www.ccdc.cam.ac.uk**). For further details, see the ESI.†

Polymerization experiments and polymer characterization

Experimental procedures in the PPR platform. All polymerization experiments were performed in a Freeslate Parallel Pressure Reactor setup with 48 reaction cells (PPR48),[50] fully contained in a triple MBraun glovebox operating under nitrogen. The cells, each with a liquid working volume of 5–6 mL, feature an 800 rpm magnetically coupled stirring, and individual online reading/control of temperature, pressure, monomer uptake, and monomer uptake rate. Experiments were carried out according to established experimental protocols[12,16,31,32,52,59,64–66] detailed below and identical to previous C_2-symmetric zirconocene catalyst screenings in propene homopolymerization[12,13,31] and copolymerization.[17]

Prior to the execution of a polymerization library, the PPR modules undergo 'bake-and-purge' cycles overnight (8 h at 90–140 °C with intermittent dry N_2 flow), to remove any contaminants and left-overs from previous experiments. After cooling to glovebox temperature, the module stir tops are taken off, and the 48 cells are fitted with disposable 10 mL glass inserts (pre-weighed in a Mettler-Toledo Bohdan Balance Automator) and stir paddles (see Table S1 for details†). The stir tops are then set back in place, and N_2 in the reactors is replaced with propene or ethene (ambient pressure). The cells are then loaded with the appropriate amounts of solvent containing TIBA as a scavenger (see Table S1 for details). For ethene/1-hexene copolymerization experiments, the desired amount of 1-hexene (Table S2.2†) is injected into the cells.

The system is then thermostated at the desired polymerization temperature and pressurized with monomer (ethene or propene, see Table S1†). At this point, the catalyst injection sequence is started; aliquots of (a) a solvent 'chaser', (b) a toluene solution of catalyst (variable amount, see Table S2.1 and S2.2†), (c) a toluene solution of the activator trityl borate or anilinium borate, variable ratio, see Table S2.1 and S2.2,† and (d) a solvent 'buffer', all separated by nitrogen gaps, are uploaded into the needle and subsequently injected into the destination cell in reverse order, thus starting the reaction. The pre-catalysts were injected into the PPR cells without pre-activation. The polymerization is left to proceed under stirring (800 rpm) at constant temperature and pressure with feed of gaseous monomer on demand until the desired monomer consumption has been reached (for reaction time, see Table S2.1 and S2.2†), and quenched by over-pressurizing the cell with 50 psi (3.4 bar) of dry air (preferred over other possible catalyst quenchers because in case of cell or quench line leakage oxygen is promptly detected by the dedicated glove-box sensor).

Polymer workup. Once all cells have been quenched, the modules are cooled down to glovebox temperature and vented, the stir-tops are removed, and the glass inserts containing the reaction phases are taken out and transferred to a centrifugal evaporator (Genevac EZ-2 Plus or Martin Christ RVC 2-33 CDplus), where all volatiles are removed, and the polymers are thoroughly dried overnight. Reaction yields are double-checked against on-line monomer conversion measurements by robotically weighing the dry polymers while still in the reaction vials, subtracting the pre-recorded tare. Polymer aliquots are then sent to the characterizations.

Polymer analytical characterizations. All polymers were characterized by means of high-temperature gel permeation chromatography (GPC) and ^{13}C NMR spectroscopy. GPC curves were recorded with a Freeslate Rapid GPC setup, equipped with a set of two mixed-bed Agilent PLgel 10 μm columns and a Polymer Char IR4 detector using *ortho*-dichlorobenzene (with 2,6-di-*tert*-butyl-4-methylphenol, BHT, added as a stabilizer, [BHT] = 0.4 mg mL^{-1}). Calibration was performed with the universal method, using ten monodisperse polystyrene samples (M_n between 1.3 and 3700 kDa). Quantitative ^{13}C NMR spectra were recorded using a Bruker Avance III 400 spectrometer equipped with a high-temperature cryoprobe for 5 mm OD tubes, on 45 mg mL^{-1} polymer solutions in tetrachloroethane-1,2-d_2 (with BHT added as a stabilizer, [BHT] = 0.4 mg mL^{-1}). Acquisition conditions were: 45° pulse; acquisition time, 2.7 s; relaxation delay, 3.3 s; 1–10 K transients. Broad-band proton decoupling was achieved with a modified WALTZ16 sequence (BI_WALTZ16_32 by Bruker).

Computational and modelling details

Precursor structures for QSPR models. Following the protocol proposed in ref. 67 dichloride metallocenes were fully opti-

mized using the Gaussian 16 software package,[68] at the TPSSTPSS[69]/cc-pVDZ(-PP)[70–73] level of theory, using a small core pseudo potential on Zr and Hf.[74–76] The protocol has been successfully used, in combination with M06-2X[77] single point energy (SP) corrections, to address several polymerization related problems: absolute barrier heights for propagation,[78] comonomer reactivity ratios,[19,20] metal–carbon bond strengths under polymerization conditions,[21–23] electronic and steric tuning of MW capability,[33] and was previously used to generate quantitative structure–property relationship (QSPR) models for stereoselectivity, regioselectivity, molar mass capability in propene polymerization and comonomer affinity in copolymerization,[12,13,16,29,31,32,40] and metal catalysed polybutadiene degradation.[79] The density fitting approximation (Resolution of Identity, RI)[80–83] and standard Gaussian16 quality settings were used at the optimization stage and SP calculations. All structures represent true minima (as indicated by the absence of imaginary frequencies). Buried volume descriptors[84] were calculated using the SambVca 2.0 program.[85] NPA charges[86,87] were determined from SP calculations at the M06-2X/cc-pVTZ(-PP) level of theory using the NBO 3.1 program,[88] implemented in Gaussian 16.

QSPR predictions. Published models for stereoselectivity, regioselectivity and molar mass capability were employed without modifications.[31] Steric and electronic descriptors were determined as detailed in ref. 31 and 13. Please note the stereoselectivity model for zirconocenes was used for legacy reasons, a more robust version not necessitating the deletion of atoms has been recently published by some of us.[29]

DFT modelling for system Ty7. All structures were fully optimized using the Gaussian 16 software package as detailed above. All structures represent either minima (as indicated by the absence of imaginary frequencies) or transition states (as indicated by one imaginary frequency corresponding to the reaction coordinate). SP energy corrections were obtained from M06-2X/cc-pVTZ(-PP) level of theory calculations.

Conflicts of interest

There are no conflicts to declare.

Acknowledgements

The authors thank Lomonosov Moscow State University Program of Development for opportunity to use NMR equipment, and Dr K. A. Lyssenko for his assistance with the X-ray structure determination analysis.

References

1 L. Resconi, L. Cavallo, A. Fait and F. Piemontesi, *Chem. Rev.*, 2000, **100**, 1253–1346.
2 V. Busico and R. Cipullo, *Prog. Polym. Sci.*, 2001, **26**, 443–533.
3 V. Busico and R. Cipullo, *J. Am. Chem. Soc.*, 1994, **116**, 9329–9330.
4 H. H. Brintzinger, D. Fischer, R. Mülhaupt, B. Rieger and R. M. Waymouth, *Angew. Chem., Int. Ed. Engl.*, 1995, **34**, 1143–1170.
5 M. K. Leclerc and H. H. Brintzinger, *J. Am. Chem. Soc.*, 1995, **117**, 1651–1652.
6 J. A. Ewen, *J. Am. Chem. Soc.*, 1984, **106**, 6355–6364.
7 J. A. Ewen, *J. Mol. Catal. A: Chem.*, 1998, **128**, 103–109.
8 V. Busico and R. Cipullo, *J. Organomet. Chem.*, 1995, **497**, 113–118.
9 M. Toto, L. Cavallo, P. Corradini, G. Moscardi, L. Resconi and G. Guerra, *Macromolecules*, 1998, **31**, 3431–3438.
10 L. Resconi, F. Piemontesi, I. Camurati, O. Sudmeijer, I. E. Nifant'ev, P. V. Ivchenko and L. G. Kuz'mina, *J. Am. Chem. Soc.*, 1998, **120**, 2308–2321.
11 G. Talarico, V. Busico and L. Cavallo, *J. Am. Chem. Soc.*, 2003, **125**, 7172–7173.
12 C. Ehm, A. Vittoria, G. P. Goryunov, P. S. Kulyabin, P. H. M. Budzelaar, A. Z. Voskoboynikov, V. Busico, D. V. Uborsky and R. Cipullo, *Macromolecules*, 2018, **51**, 8073–8083.
13 P. S. Kulyabin, G. P. Goryunov, M. I. Sharikov, V. V. Izmer, A. Vittoria, P. H. M. Budzelaar, V. Busico, A. Z. Voskoboynikov, C. Ehm, R. Cipullo and D. V. Uborsky, *J. Am. Chem. Soc.*, 2021, **143**, 7641–7647.
14 V. Busico, R. Cipullo, F. Cutillo, N. Friederichs, S. Ronca and B. Wang, *J. Am. Chem. Soc.*, 2003, **125**, 12402–12403.
15 G. Urciuoli, F. Zaccaria, C. Zuccaccia, R. Cipullo, P. H. M. Budzelaar, A. Vittoria, C. Ehm, A. Macchioni and V. Busico, *Polymers*, 2023, **15**, 1378.
16 D. V. Uborsky, D. Y. Mladentsev, B. A. Guzeev, I. S. Borisov, A. Vittoria, C. Ehm, R. Cipullo, C. Hendriksen, N. Friederichs, V. Busico and A. Z. Voskoboynikov, *Dalton Trans.*, 2020, **49**, 3015–3025.
17 C. Ehm, A. Vittoria, G. P. Goryunov, V. V. Izmer, D. S. Kononovich, O. V. Samsonov, P. H. M. Budzelaar, A. Z. Voskoboynikov, V. Busico, D. V. Uborsky and R. Cipullo, *Dalton Trans.*, 2020, **49**, 10162–10172.
18 N. Friederichs, B. Wang, P. H. M. Budzelaar and B. B. Coussens, *J. Mol. Catal. A: Chem.*, 2005, **242**, 91–104.
19 F. Zaccaria, C. Ehm, P. H. M. Budzelaar and V. Busico, *ACS Catal.*, 2017, **7**, 1512–1519.
20 F. Zaccaria, R. Cipullo, P. H. M. Budzelaar, V. Busico and C. Ehm, *J. Polym. Sci., Part A: Polym. Chem.*, 2017, **55**, 2807–2814.
21 C. Ehm, P. H. M. Budzelaar and V. Busico, *J. Catal.*, 2017, **351**, 146–152.
22 C. Ehm, R. Cipullo, M. Passaro, F. Zaccaria, P. H. M. Budzelaar and V. Busico, *ACS Catal.*, 2016, **6**, 7989–7993.
23 F. Zaccaria, C. Ehm, P. H. M. Budzelaar, V. Busico and R. Cipullo, *Organometallics*, 2018, **37**, 2872–2879.
24 F. Zaccaria, C. Zuccaccia, R. Cipullo, P. H. M. Budzelaar, A. Macchioni, V. Busico and C. Ehm, *Organometallics*, 2018, **37**, 4189–4194.

25 R. Cipullo, P. Melone, Y. Yu, D. Iannone and V. Busico, *Dalton Trans.*, 2015, **44**, 12304–12311.
26 P. A. Wilson, M. H. Hannant, J. A. Wright, R. D. Cannon and M. Bochmann, *Macromol. Symp.*, 2006, **236**, 100–110.
27 M. Bochmann, *Organometallics*, 2010, **29**, 4711–4740.
28 D. V. Uborsky, M. I. Sharikov, G. P. Goryunov, K. M. Li, A. Dall'Anese, C. Zuccaccia, A. Vittoria, T. Iovine, G. Galasso, C. Ehm, A. Macchioni, V. Busico, A. Z. Voskoboynikov and R. Cipullo, *Inorg. Chem. Front.*, 2023, **10**, 6401–6406.
29 G. Antinucci, B. Dereli, A. Vittoria, P. H. M. Budzelaar, R. Cipullo, G. P. Goryunov, P. S. Kulyabin, D. V. Uborsky, L. Cavallo, C. Ehm, A. Z. Voskoboynikov and V. Busico, *ACS Catal.*, 2022, **12**, 6934–6945.
30 A. Poater and L. Cavallo, *Dalton Trans.*, 2009, 8885–8890.
31 C. Ehm, A. Vittoria, P. G. Goryunov, V. V. Izmer, S. D. Kononovich, V. O. Samsonov, R. Di Girolamo, H. M. P. Budzelaar, Z. A. Voskoboynikov, V. Busico, V. D. Uborsky and R. Cipullo, *Polymers*, 2020, **12**, 1005–1005.
32 C. Ehm, A. Vittoria, G. P. Goryunov, V. V. Izmer, D. S. Kononovich, P. S. Kulyabin, R. Di Girolamo, P. H. M. Budzelaar, A. Z. Voskoboynikov, V. Busico, D. V. Uborsky and R. Cipullo, *Macromolecules*, 2020, **53**, 9325–9336.
33 C. Ehm, P. H. M. Budzelaar and V. Busico, *Eur. J. Inorg. Chem.*, 2017, **2017**, 3343–3349.
34 C. I. Branden and J. Tooze, *Introduction to Protein Structure*, Garland Publishing, New York, 1990–1991.
35 J. Kyte, *Structure in Protein Chemistry*, Garland Publishing, New York, 1995.
36 J.-M. Lehn, *Angew. Chem., Int. Ed. Engl.*, 1988, **27**, 89–112.
37 A. Schöbel, E. Herdtweck, M. Parkinson and B. Rieger, *Chem. – Eur. J.*, 2012, **18**, 4174–4178.
38 M. R. Machat, D. Lanzinger, A. Pöthig and B. Rieger, *Organometallics*, 2017, **36**, 399–408.
39 G. P. Goryunov, M. I. Sharikov, A. N. Iashin, J. A. M. Canich, S. J. Mattler, J. R. Hagadorn, D. V. Uborsky and A. Z. Voskoboynikov, *ACS Catal.*, 2021, **11**, 8079–8086.
40 A. Vittoria, G. P. Goryunov, V. V. Izmer, D. S. Kononovich, O. V. Samsonov, F. Zaccaria, G. Urciuoli, P. H. M. Budzelaar, V. Busico, A. Z. Voskoboynikov, D. V. Uborsky, C. Ehm and R. Cipullo, *Polymers*, 2021, **13**, 2621.
41 C. Cobzaru, S. Hild, A. Boger, C. Troll and B. Rieger, *Coord. Chem. Rev.*, 2006, **250**, 189–211.
42 T. Fillebeen, T. Hascall and G. Parkin, *Inorg. Chem.*, 1997, **36**, 3787–3790.
43 C. Azerraf, O. Grossman and D. Gelman, *J. Organomet. Chem.*, 2007, **692**, 761–767.
44 O. Grossman, C. Azerraf and D. Gelman, *Organometallics*, 2006, **25**, 375–381.
45 A. Kaps and H. Plenio, *Eur. J. Inorg. Chem.*, 2023, **26**, e202300178.
46 S. Barman, E. A. Jaseer, N. Garcia, M. Elanany, M. Khawaji, W. Xu, S. Lin, H. Alasiri, M. N. Akhtar and R. Theravalappil, *Chem. Commun.*, 2022, **58**, 10044–10047.
47 P. S. Kulyabin, V. V. Izmer, G. P. Goryunov, M. I. Sharikov, D. S. Kononovich, D. V. Uborsky, J. A. M. Canich and A. Z. Voskoboynikov, *Dalton Trans.*, 2021, **50**, 6170–6180.
48 W. Kaminsky, O. Rabe, A. M. Schauwienold, G. U. Schupfner, J. Hanss and J. Kopf, *J. Organomet. Chem.*, 1995, **497**, 181–193.
49 J.-C. Buffet, T. A. Q. Arnold, Z. R. Turner, P. Angpanitcharoen and D. O'Hare, *RSC Adv.*, 2015, **5**, 87456–87464.
50 V. Murphy, X. Bei, T. R. Boussie, O. Brümmer, G. M. Diamond, C. Goh, K. A. Hall, A. M. Lapointe, M. Leclerc, J. M. Longmire, J. A. W. Shoemaker, H. Turner and W. H. Weinberg, *Chem. Rec.*, 2002, **2**, 278–289.
51 T. R. Boussie, G. M. Diamond, C. Goh, K. A. Hall, A. M. LaPointe, M. Leclerc, C. Lund, V. Murphy, J. A. W. Shoemaker, U. Tracht, H. Turner, J. Zhang, T. Uno, R. K. Rosen and J. C. Stevens, *J. Am. Chem. Soc.*, 2003, **125**, 4306–4317.
52 C. Ehm, A. Mingione, A. Vittoria, F. Zaccaria, R. Cipullo and V. Busico, *Ind. Eng. Chem. Res.*, 2020, **59**, 13940–13947.
53 W. Kaminsky, *Macromol. Chem. Phys.*, 1996, **197**, 3907–3945.
54 U. Stehling, J. Diebold, R. Kirsten, W. Roell, H. H. Brintzinger, S. Juengling, R. Muelhaupt and F. Langhauser, *Organometallics*, 1994, **13**, 964–970.
55 I. E. Nifant'ev, P. V. Ivchenko, V. V. Bagrov, A. V. Churakov and P. Mercandelli, *Organometallics*, 2012, **31**, 4962–4970.
56 K. Reichelt, M. Parkinson and L. Resconi, *Macromol. Chem. Phys.*, 2016, **217**, 2415–2430.
57 M. S. Kuklin, V. Virkkunen, P. M. Castro, L. Resconi and M. Linnolahti, *Eur. J. Inorg. Chem.*, 2015, **2015**, 4420–4428.
58 D. Tranchida and L. Resconi, *Polym. Cryst.*, 2018, **1**, e10022.
59 A. Vittoria, A. Meppelder, N. Friederichs, V. Busico and R. Cipullo, *ACS Catal.*, 2017, **7**, 4509–4518.
60 E. Alcalde, N. Mesquida, J. Frigola, S. López-Pérez and R. Mercè, *Org. Biomol. Chem.*, 2008, **6**, 3795–3810.
61 *SAINT Plus*. Bruker AXS Inc., Madison, Wisconsin, USA, 2012.
62 G. Sheldrick, *Acta Crystallogr., Sect. A: Found. Crystallogr.*, 2008, **64**, 112–122.
63 G. Sheldrick, *Acta Crystallogr., Sect. E: Crystallogr. Commun.*, 2015, **71**, 3–8.
64 A. Vittoria, V. Busico, F. D. Cannavacciuolo and R. Cipullo, *ACS Catal.*, 2018, **8**, 5051–5061.
65 A. Vittoria, A. Mingione, R. A. Abbate, R. Cipullo and V. Busico, *Ind. Eng. Chem. Res.*, 2019, **58**, 14729–14735.
66 A. Vittoria, A. Meppelder, N. Friederichs, V. Busico and R. Cipullo, *ACS Catal.*, 2020, **10**, 644–651.
67 C. Ehm, P. H. M. Budzelaar and V. Busico, *J. Organomet. Chem.*, 2015, **775**, 39–49.
68 M. J. Frisch, G. W. Trucks, H. B. Schlegel, G. E. Scuseria, M. A. Robb, J. R. Cheeseman, G. Scalmani, V. Barone, G. A. Petersson, H. Nakatsuji, X. Li, M. Caricato, A. V. Marenich, J. Bloino, B. G. Janesko, R. Gomperts, B. Mennucci, H. P. Hratchian, J. V. Ortiz, A. F. Izmaylov, J. L. Sonnenberg, D. Williams-Young, F. Ding, F. Lipparini,

F. Egidi, J. Goings, B. Peng, A. Petrone, T. Henderson, D. Ranasinghe, V. G. Zakrzewski, J. Gao, N. Rega, G. Zheng, W. Liang, M. Hada, M. Ehara, K. Toyota, R. Fukuda, J. Hasegawa, M. Ishida, T. Nakajima, Y. Honda, O. Kitao, H. Nakai, T. Vreven, K. Throssell, J. A. Montgomery Jr., J. E. Peralta, F. Ogliaro, M. J. Bearpark, J. J. Heyd, E. N. Brothers, K. N. Kudin, V. N. Staroverov, T. A. Keith, R. Kobayashi, J. Normand, K. Raghavachari, A. P. Rendell, J. C. Burant, S. S. Iyengar, J. Tomasi, M. Cossi, J. M. Millam, M. Klene, C. Adamo, R. Cammi, J. W. Ochterski, R. L. Martin, K. Morokuma, O. Farkas, J. B. Foresman and D. J. Fox, *Gaussian 16, Revision A.03*, Gaussian, Inc., Wallingford CT, 2016.

69 J. M. Tao, J. P. Perdew, V. N. Staroverov and G. E. Scuseria, *Phys. Rev. Lett.*, 2003, **91**, 146401.

70 N. B. Balabanov and K. A. Peterson, *J. Chem. Phys.*, 2005, **123**, 064107.

71 N. B. Balabanov and K. A. Peterson, *J. Chem. Phys.*, 2006, **125**, 074110.

72 K. L. Schuchardt, B. T. Didier, T. Elsethagen, L. Sun, V. Gurumoorthi, J. Chase, J. Li and T. L. Windus, *J. Chem. Inf. Model.*, 2007, **47**, 1045–1052.

73 B. P. Pritchard, D. Altarawy, B. Didier, T. D. Gibson and T. L. Windus, *J. Chem. Inf. Model.*, 2019, **59**, 4814–4820.

74 P. Schwerdtfeger, *ChemPhysChem*, 2011, **12**, 3143–3155.

75 K. A. Peterson, D. Figgen, M. Dolg and H. Stoll, *J. Chem. Phys.*, 2007, **126**, 124101.

76 D. Figgen, K. A. Peterson, M. Dolg and H. Stoll, *J. Chem. Phys.*, 2009, **130**, 164108.

77 Y. Zhao and D. G. Truhlar, *Theor. Chem. Acc.*, 2007, **120**, 215–241.

78 C. Ehm, R. Cipullo, P. H. M. Budzelaar and V. Busico, *Dalton Trans.*, 2016, **45**, 6847–6855.

79 F. D. Cannavacciuolo, R. Yadav, A. Esper, A. Vittoria, G. Antinucci, F. Zaccaria, R. Cipullo, P. H. M. Budzelaar, V. Busico, G. P. Goryunov, D. V. Uborsky, A. Z. Voskoboynikov, K. Searles, C. Ehm and A. S. Veige, *Angew. Chem., Int. Ed.*, 2022, e202202258.

80 J. L. Whitten, *J. Chem. Phys.*, 1973, **58**, 4496.

81 E. J. Baerends, D. E. Ellis and P. Ros, *Chem. Phys.*, 1973, **2**, 41–51.

82 M. Feyereisen, G. Fitzgerald and A. Komornicki, *Chem. Phys. Lett.*, 1993, **208**, 359–363.

83 O. Vahtras, J. Almlöf and M. W. Feyereisen, *Chem. Phys. Lett.*, 1993, **213**, 514–518.

84 L. Falivene, Z. Cao, A. Petta, L. Serra, A. Poater, R. Oliva, V. Scarano and L. Cavallo, *Nat. Chem.*, 2019, **11**, 872–879.

85 L. Falivene, R. Credendino, A. Poater, A. Petta, L. Serra, R. Oliva, V. Scarano and L. Cavallo, *Organometallics*, 2016, **35**, 2286–2293.

86 F. Weinhold and C. R. Landis, *Valence and Bonding - A Natural Bond Orbital Donor-Acceptor Perspective*, Cambridge University Press, Cambridge, UK, 2005.

87 E. D. Glendening, C. R. Landis and F. Weinhold, *Wiley Interdiscip. Rev. Comput. Mol. Sci*, 2012, 2, 1–42.

88 *Theoretical Chemistry Institute*, ed. E. D. Glendening, A. E. Reed, J. E. Carpenter, F. Weinhold and NBO 3.1, University of Wisconsin, Madison, WI, 2001.